Available online at www.sciencedirect.com
ScienceDirect
Journal of Sound and Vibration 305 (2007) 378–400
JOURNAL OF SOUND AND VIBRATION
www.elsevier.com/locate/jsvi

Dynamic instability of supercritical driveshafts mounted on dissipative supports—Effects of viscous and hysteretic internal damping

O. Montagnier[a,*], Ch. Hochard[b]

[a]Centre de Recherche de l'Armée de l'Air (CReA), Laboratoire de Dynamique du Vol, BA 701, 13361 Salon Air, France
[b]Laboratoire de Mécanique et d'Acoustique (LMA), 31 chemin Joseph Aiguier, 13402 Marseille Cedex 20, France

Received 8 December 2006; received in revised form 6 March 2007; accepted 22 March 2007
Available online 5 July 2007

Abstract

The case of a rotating shaft with internal damping mounted either on elastic dissipative bearings or on infinitely rigid bearings with viscoelastic suspensions is investigated in order to obtain the stability region. A Euler–Bernoulli shaft model is adopted, in which the transverse shear effects are neglected and the effects of translational and rotatory inertia, gyroscopic moments, and internal viscous or hysteretic damping are taken into account. The hysteretic damping is incorporated with an equivalent viscous damping coefficient. Free motion analysis yields critical speeds and threshold speeds for each damping model in analytical form. In the case of elastic dissipative bearings, the present results are compared with the results of previous studies on finite element models. In the case of infinitely rigid bearings with viscoelastic suspensions, it is established that viscoelastic supports increase the stability of long shafts, thus compensating for the loss of efficiency which occurs with classical bearings. The instability criteria also show that the effect of the coupling which occured between rigid modes introducing external damping and shaft modes are almost more important than damping factor. Lastly, comparisons between viscous and hysteretic damping conditions lead to the conclusion that an appropriate material damping model is essential to be able to assess these instabilities.
© 2007 Published by Elsevier Ltd.

1. Introduction

The use of driveshafts in the supercritical range has proved to be of great interest for many applications, especially those involving long drivelines (helicopters, tiltrotors, etc.). However, in the field of rotordynamics, internal damping, which is also called rotating damping, is known to cause whirl instabilities in this speed range. In particular, with long driveshafts consisting of materials which are more dissipative than metallic materials (such as some carbon/epoxy laminates [1]), these instabilities tend to occur more frequently. The aim of the present study was to develop a theoretical model for determining these instabilities and to establish the most decisive parameters.

*Corresponding author. Tel.: +33 04 90 17 80 93; fax: +33 04 90 17 81 89.
E-mail address: olivier.montagnier@air.defense.gouv.fr (O. Montagnier).

0022-460X/$ - see front matter © 2007 Published by Elsevier Ltd.
doi:10.1016/j.jsv.2007.03.061

Nomenclature

a	shear strain parameter
c	viscous damping
d	modal damping
E, G	Young's modulus and shear modulus of the shaft
I	mass moment of inertia $/\vec{y}$ or $/\vec{z}$ per unit mass density and unit length equal to the diametrical cross-section of inertia
i	imaginary unit $\sqrt{-1}$
J	mass moment of inertia $/\vec{x}$ per unit mass density and unit length
k	stiffness
l	length of the shaft
m	mass
$(o,\vec{x},\vec{y},\vec{z})$	fixed frame of reference
$(O,\vec{x},\vec{Y},\vec{Z})$	rotational frame of reference
r	shaft radius
S	cross-section area of the shaft
u	complex displacement
U	complex amplitude of the complex displacement u
ε	distance between the sectional centre of inertia and the shaft theoretical axis without deformations
η	loss factor
θ	complex rotation
Θ	complex amplitude of the complex rotation θ
κ	shear coefficient
λ	complex frequency of the rotor
μ	viscous loss factor
ρ	density of the shaft
Ω	spin speed
ω_{b1}	natural frequency of the cylindrical rigid-body mode (infinitely rigid shaft)
ω_{b2}	natural frequency of the conical rigid-body mode (infinitely rigid shaft)
ω_{sn}	nth natural frequency of a beam with constant cross-section in bending, simply supported at both ends

Subscript

$B-$, $B+$	lower and higher backward speeds
b	bearing
c	critical
e	external
eq	equivalent
$F-$, $F+$	lower and higher forward speeds
hyst	hysteretic model
i	internal
ths	threshold speed
p	$(\in \{B-, B+, F-, F+\})$
n	number of the sine mode or number of the harmonic $(\in \mathbb{N}^*)$
s	shaft
sub	subcritical
sup	supercritical
visc	viscous model
0	gyroscopic effects assumed to be negligible $(\Gamma_n \approx 0)$

In the field of rotordynamic, internal damping is generally treated like viscous damping, because this parameter can easily be introduced into rotor equations, and because viscous damping is reasonably realistic to simulate external dissipation (roller bearings, hydrodynamic bearings, etc.). However, most materials are known to show vibratory damping behaviour which resembles hysteretic damping much more than viscous damping, as in the case of metallic materials [2], carbon/epoxy materials [1] and in a more approximate way, viscoelastic materials such as elastomers [3]. The main characteristics of hysteretic damping are as follows: the corresponding hysteresis loop (stress–strain loop) is independent of the excitation frequency; the cyclic energy dissipation is independent of the excitation frequency and proportional to the square of the deflection amplitude. In classical vibration mechanics, hysteretic damping is often used and generally introduced using the complex stiffness. However, in rotordynamics, it is difficult to introduce complex stiffness into the rotating reference frame except in some particular cases (such as that of forced motion [4]). In most cases, it is therefore necessary to use an equivalent viscous damping coefficient. This procedure still requires some care to be taken because of the multi-frequency excitation. In particular, whirl speeds in the rotating reference frame differ from those occuring in the fixed reference frame. Wettergren has shown both theoretically and experimentally that these hysteretic damping factors can be replaced by the equivalent viscous damping even when multi-frequencies are involved [5]. The equations can therefore be treated using a

classical approach with an internal viscous damping term. An equivalent coefficient is then introduced into the modal solutions.

Here it is proposed to show the differences between the stability results obtained with internal viscous damping and internal hysteretic damping models, in the particular case of a continuous symmetrical dissipative shaft without any disk. Since external damping is necessary to obtain a stable range in supercritical motion, two cases are studied: a shaft mounted on elastic dissipative bearings, and a shaft with infinitely rigid bearings mounted on viscoelastic supports.

In the first part, a Euler–Bernoulli beam model is adopted, which neglects the transverse shear effects but takes the effects of translational and rotatory inertia, gyroscopic moments, and internal viscous or hysteretic damping into account. Free motion analysis gives critical speeds and instability criteria for each damping model in an analytical form. In the literature, these instabilities due to internal damping have generally been obtained numerically using finite elements methods. The case of viscous damping can easily be dealt with using finite elements methods, whereas the case of hysteretic damping is not so straightforward, and has given rise to several errors in the literature which were collected by Genta [6]. Note that Genta himself has proposed a finite element model that accounts satisfactorily for hysteretic internal damping [7]. The main advantages of analytical solutions compared to numerical results are that they give a better control over parameters affecting the stability, and a better understanding of instability processes, and that they lend themselves to extremely fast implementation for optimization computations. Analytical solutions also provide reference data, which can be used in particular to check the validity of finite element models including hysteretic internal damping. On the other hand, finite element computations are suitable for studing more complex rotor configurations.

In the second part of this paper, three applications of results presented in the first part will be described. In the first case study, the validity of the model is confirmed by comparing the solutions obtained with data previously published in the literature which were obtained using various finite element models including a viscous internal damping parameter. The second case study deals with the effects of hysteretic damping. Lastly, to determine the effects of the viscoelastic supports, comparisons are made between the two shaft configurations.

2. Axisymmetric elastic shaft model with internal damping

When operating rotors in the supercritical range, it is necessary to introduce external damping to reduce the unbalanced vibration response amplitudes and to increase the stability. Since classical rolling-element bearings and hydrodynamic bearings do not generally provide sufficient damping, additional squeeze-film dampers are generally fitted. The main disadvantages of these bearing supports are the complexity of their installation, their limited operational range and their high cost [3]. Another means of increasing the external damping consists in adding dampers directly between the shaft and the fixed frame [8]. Lastly, an economic solution, which has been developing during the last few years, consists in adding viscoelastic materials such as elastomers between the bearing and the fixed framework. Kirk and Gunter have established that these viscoelastic supports improve the stability domain of the disk-shaft system [9]. In a study on the stability of a Jeffcott rotor with elastic linear bearings mounted on viscoelastic supports and with an undamped elastic non-massive shaft, Dutt and Nakra showed that by choosing the viscoelastic supports appropriately, it is possible to greatly increase the stability domain of the system [10]. In another paper, these authors reported that the unbalanced responses of the same system were greatly reduced by incorporating suitable viscoelastic supports [11]. Shabaneh and Zu studied a Jeffcott rotor with elastic dissipative bearings mounted on viscoelastic supports, assuming the shaft to be elastic, massive and viscously damped [12]. Based on a Timoshenko beam theory and a hysteretic damping model for the viscoelastic supports, they obtained similar effects on unbalanced responses. Note that in all these studies, the shaft damping is always assumed to be viscous.

This part of the paper focuses on two very similar shaft configurations in terms of their equations. The first configuration consists of a shaft mounted on flexible bearings which are assumed to be elastic and viscously damped (Fig. 1). The second one consists of a shaft mounted on infinitely rigid bearings with viscoelastic supports assumed to show complex stiffness, i.e. to be elastic and hystereticly damped (Fig. 2). The two shaft

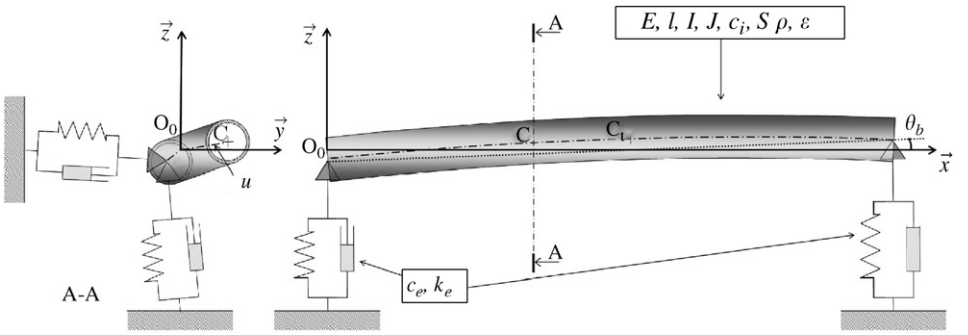

Fig. 1. Configuration 1: elastic shaft mounted on flexible dissipative bearings.

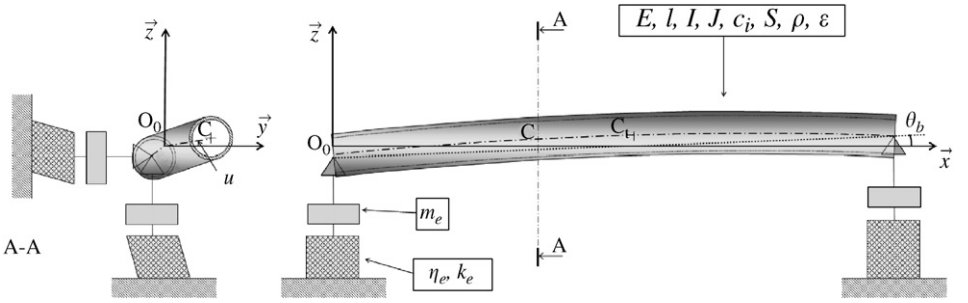

Fig. 2. Configuration 2: elastic shaft mounted on infinitely rigid massive bearings on viscoelastic supports.

configurations are governed by the same equations, only the mass of the bearings has to be added in the second configuration.

We take a symmetric elastic shaft supported at both ends, as shown in Figs. 1 and 2, where $(O, \vec{x}, \vec{y}, \vec{z})$ is the inertial frame. A Euler–Bernoulli beam theory is adopted: this theory is applicable to slender shafts, i.e. shafts with a small diameter in comparison with their length, approximately $l/r > 10$. The Timoshenko beam theory is useful if the shear strains are large, i.e. in the case of a stubby shaft or in the presence of disks. The shaft is defined by its Young's modulus E, its length l, its radius r and its mass density ρ. When the damping is assumed to be hysteretic, it is defined by its loss factor η_i, but for convenience, it is necessary to define an internal viscous damping term per unit length c_i. The gyroscopic effect of the shaft is taken into account. The eccentricity of a shaft section is given by the function $\varepsilon(x)$. This function defines the distance between the sectional centre of inertia and the theoretical axis of the shaft without any deformations with $x \in [0, l]$. Gravity is neglected.

In the case of configuration 1, the isotropic bearing is modelled by a Kelvin–Voigt model consisting of a stiffness parameter k_e $(= k_{yy} = k_{zz})$ and a viscous damping parameter c_e $(= c_{yy} = c_{zz})$. In the case of configuration 2, each axisymmetric bearing, which is assumed to be infinitely rigid, is represented by its mass m_e, and each isotropic elastomer support is represented by a complex stiffness model consisting of a stiffness k_e $(= k_{yy} = k_{zz})$ and a loss factor η_e $(= \eta_{yy} = \eta_{zz})$. In the latter case, for convenience, an external viscous damping term c_e will be used in the equations.

Subsequently, displacements will be expressed in complex form. The rigid-body motion (unstrained shaft) consists in a displacement parallel to the $O_0\vec{x}$ axis and a rotation around the unstrained shaft centre C_t. This displacement and this rotation are denoted u_b $(= u_{by} + \mathrm{i}u_{bz})$ and θ_b $(= \theta_{by} + \mathrm{i}\theta_{bz})$, respectively. The deflection of the shaft section centres C consists of a displacement relative to the unstrained shaft axle and is denoted u_s $(= u_{sy} + \mathrm{i}u_{sz})$. With these notations, the cross-sectional displacement, i.e. the displacement of C relative to the fixed frame is:

$$u(x,t) = u_b(t) + \left(x - \frac{l}{2}\right)\theta_b(t) + u_s(x,t). \tag{1}$$

The boundary conditions in terms of the displacement are: one null moment when $x = \{0, l\}$; one null displacement between the shaft and the bearing when $x = \{0, l\}$. These conditions are expressed as follows:

$$u_s''(0,t) = 0, \quad u_s''(l,t) = 0, \quad u_s(0,t) = 0, \quad u_s(l,t) = 0, \tag{2}$$

where $()' = \partial/\partial x$. Based on the above assumptions and without any internal damping, the local governing equation of motion for the shaft is classically [7]:

$$\ddot{u} - \frac{I}{S}\ddot{u}'' + \mathrm{i}\Omega\frac{J}{S}\dot{u}'' + \frac{EI}{\rho S}u'''' = \varepsilon(x)\Omega^2\mathrm{e}^{\mathrm{i}\Omega t} \quad \forall x \in [0,l], \tag{3}$$

where $(\cdot) = \partial/\partial t$, S is the cross-section area of the shaft, I is the mass moment of inertia $/\vec{y}$ or $/\vec{z}$ per unit mass density and unit length equivalent to the diametric cross-section of inertia, J is the polar moment of inertia $/\vec{x}$ per unit mass density and unit length, and Ω is the spin speed. Internal damping is introduced into this equation, noting that this dissipation appears in the rotational frame, and that it is relative to the variable u_s and not u. In that case, since $u'''' = u_s''''$, the local governing equation of motion for the shaft with internal damping is

$$\ddot{u} - \frac{I}{S}\ddot{u}'' + \mathrm{i}\Omega\frac{J}{S}\dot{u}'' + \frac{EI}{\rho S}u_s'''' + \frac{c_i}{\rho S}(\dot{u}_s - \mathrm{i}\Omega u_s) = \varepsilon(x)\Omega^2\mathrm{e}^{\mathrm{i}\Omega t} \qquad \forall x \in [0,l]. \tag{4}$$

Finally, the boundary conditions give two supplementary equations of motion corresponding to the equilibrium of the shaft-bearings system in terms of force and moment:

$$\int_0^l \rho S\ddot{u}\,\mathrm{d}x + 2m_e\ddot{u}_b + 2c_e\dot{u}_b + 2k_e u_b = \int_0^l \rho S\varepsilon(x)\Omega^2\mathrm{e}^{\mathrm{i}\Omega t}\,\mathrm{d}x, \tag{5}$$

$$\int_0^l \rho S\left(x - \frac{l}{2}\right)\ddot{u}\,\mathrm{d}x + 2m_e\frac{l^2}{4}\ddot{\theta}_b + 2c_e\frac{l^2}{4}\dot{\theta}_b + 2k_e\frac{l^2}{4}\theta_b = \int_0^l \rho S\left(x - \frac{l}{2}\right)\varepsilon(x)\Omega^2\mathrm{e}^{\mathrm{i}\Omega t}\,\mathrm{d}x. \tag{6}$$

Studies on the unbalanced motion of this system have been presented in Refs. [13,14]. Let us therefore note that by defining the stationary whirl $\dot{u}_s = \mathrm{i}\Omega u_s$ and according to Eq. (4), the internal damping has no effect.

Studies on the free motion corresponding to solving the characteristic equation are not usually carried out using analytical methods. The equations of interest here are the above Eqs. (4)–(6) without the second member:

$$\begin{cases} \ddot{u} - \dfrac{I}{S}\ddot{u}'' + \mathrm{i}\Omega\dfrac{J}{S}\dot{u}'' + \dfrac{EI}{\rho S}u_s'''' + \dfrac{c_i}{\rho S}(\dot{u}_s - \mathrm{i}\Omega u_s) = 0 \quad \forall x \in [0,l], & (7) \\ \int_0^l \rho S\ddot{u}\,\mathrm{d}x + 2m_e\ddot{u}_b + 2c_e\dot{u}_b + 2k_e u_b = 0, & (8) \\ \int_0^l \rho S\left(x - \dfrac{l}{2}\right)\ddot{u}\,\mathrm{d}x + 2m_e\dfrac{l^2}{4}\ddot{\theta}_b + 2c_e\dfrac{l^2}{4}\dot{\theta}_b + 2k_e\dfrac{l^2}{4}\theta_b = 0. & (9) \end{cases}$$

The shaft mode shapes are assumed to be proportional to the sinusoid function. Therefore, the displacements and rotations, with the harmonic $n \in \mathbb{N}^*$, can be expressed as follows:

$$u_s(x,t) = U_{sn}\sin\left(\frac{\pi n x}{l}\right)\mathrm{e}^{\mathrm{i}\lambda_n t}, \quad u_b(t) = U_{bn}\mathrm{e}^{\mathrm{i}\lambda_n t}, \quad \theta_b(t) = \Theta_{bn}\mathrm{e}^{\mathrm{i}\lambda_n t}, \tag{10}$$

where U_{sn}, U_{bn} are complex displacements, Θ_{bn} are complex rotations, and λ_n are complex eigenvalues. The virtual work principle is applied and this yields weak formulation starting with the strong formulation Eq. (7):

$$\forall u^* \in \mathrm{KA}_0 \int_0^l \left[\ddot{u} - \frac{I}{S}\ddot{u}'' + \mathrm{i}\Omega\frac{J}{S}\dot{u}'' + \frac{EI}{\rho S}u_s'''' + \frac{c_i}{\rho S}(\dot{u}_s - \mathrm{i}\Omega u_s)\right]u^*\,\mathrm{d}x = 0. \tag{11}$$

The kinematically admissible (KA_0) displacement field is taken in the following form:

$$u^* = \sin\left(\frac{\pi n x}{l}\right)\mathrm{e}^{\mathrm{i}\lambda_n t}. \tag{12}$$

Substituting Eqs. (10) and (12) into the equations of motion (8), (9) and (11) yields, after some calculations:

$$\begin{cases} [-\Pi_n\lambda_n^2+\Gamma_n\Omega\lambda_n+\mathrm{i}d_{in}(\lambda_n-\Omega)+\omega_{sn}^2]U_{sn}-\lambda_n^2\dfrac{2}{n\pi}\left[(1-(-1)^n)U_{bn}-(1+(-1)^n)\dfrac{l}{2}\Theta_{bn}\right]=0,\\ -\Phi_1\lambda_n^2\dfrac{(1-(-1)^n)}{2n\pi}U_{sn}+[-\lambda_n^2+d_{e1}\mathrm{i}\lambda_n+\omega_{b1}^2]U_{bn}=0,\\ \Phi_2\lambda_n^2\dfrac{(1+(-1)^n)}{2n\pi}U_{sn}+[-\lambda_n^2+d_{e2}\mathrm{i}\lambda_n+\omega_{b2}^2]\dfrac{l}{2}\Theta_{bn}=0, \end{cases} \tag{13}$$

with

$$\omega_{sn}^2=\frac{EI}{\rho S}\left(\frac{\pi n}{l}\right)^4=\frac{k_{sn}}{m_s},\quad \omega_{bn}^2=\frac{k_e}{m_e+\dfrac{m_s}{2(2+(-1)^n)}},\quad d_{en}=\frac{c_e}{m_e+\dfrac{m_s}{2(2+(-1)^n)}},$$
$$d_{in}=\frac{c_i}{\rho S},\quad \Phi_n=\frac{m_s}{m_e+\dfrac{m_s}{2(2+(-1)^n)}},\quad \Pi_n=1+\frac{I}{S}\left(\frac{\pi n}{l}\right)^2,\quad \Gamma_n=\frac{J}{S}\left(\frac{\pi n}{l}\right)^2, \tag{14}$$

where ω_{sn} is the nth natural frequency of the shaft without any coupling effects (the exact eigenvalue of a beam with a constant cross-section in bending, which is simply supported at both ends), k_{sn} is the nth modal stiffness of the shaft, ω_{b1} and ω_{b2} are the two natural frequencies of the rigid-body modes without any coupling effects (the shaft is assumed infinitely rigid), d_{en} and d_{in} are the nth external and internal viscous damping parameters per unit mass, and Φ_n is a ratio of mass between the mass of the shaft m_s and the mass of the bearings. Therefore, if n is an odd number, by replacing suffix 1 by n, the system (13) can be expressed as follows:

$$\begin{cases} [-\Pi_n\lambda_n^2+\Gamma_n\Omega\lambda_n+\mathrm{i}d_{in}(\lambda_n-\Omega)+\omega_{sn}^2]U_{sn}=\lambda_n^2\dfrac{4}{n\pi}U_{bn},\\ [-\lambda_n^2+d_{en}\mathrm{i}\lambda_n+\omega_{bn}^2]U_{bn}=\dfrac{\Phi_n}{n\pi}\lambda_n^2U_{tn},\\ \Theta_{bn}=0. \end{cases} \tag{15}$$

If n is an even number, by replacing suffix 2 by n, the system (13) can be expressed as follows:

$$\begin{cases} [-\Pi_n\lambda_n^2+\Gamma_n\Omega\lambda_n+\mathrm{i}d_{in}(\lambda_n-\Omega)+\omega_{sn}^2]U_{sn}=-\lambda_n^2\dfrac{4}{n\pi}\dfrac{l}{2}\Theta_{bn},\\ U_{bn}=0,\\ [-\lambda_n^2+d_{en}\mathrm{i}\lambda_n+\omega_{bn}^2]\dfrac{l}{2}\Theta_{bn}=-\dfrac{\Phi_n}{n\pi}\lambda_n^2U_{sn}. \end{cases} \tag{16}$$

The two previous systems have an equivalent form and can be expressed as a single characteristic fourth-order equation in terms of λ_n, which is suitable for all $n\in\mathbb{N}^*$:

$$\begin{aligned}\Psi_n\lambda_n^4-[\Gamma_n\Omega+\mathrm{i}(\Pi_nd_{en}+d_{in})]\lambda_n^3-[\omega_{sn}^2+\Pi_n\omega_{bn}^2+d_{in}d_{en}-\mathrm{i}\Omega(\Gamma_nd_{en}+d_{in})]\lambda_n^2\\ +[(\Gamma_n\omega_{bn}^2+d_{in}d_{en})\Omega+\mathrm{i}(d_{in}\omega_{bn}^2+d_{en}\omega_{sn}^2)]\lambda_n+(\omega_{sn}^2-\mathrm{i}d_{in}\Omega)\omega_{bn}^2=0,\end{aligned} \tag{17}$$

with

$$\Psi_n=\Pi_n-\frac{4}{n^2\pi^2}\Phi_n. \tag{18}$$

Let us express the eigenvalue solutions in complex form as follows:

$$\lambda_n=\omega_n+\mathrm{i}d_n. \tag{19}$$

The real part ω_n and the imaginary part d_n are an angular frequency term and a modal damping term, respectively. Hence, assuming weak damping to occur in the rotor-system yields $\omega_n\gg d_n$. It will be assumed below that the angular frequencies are large in comparison with the modal damping, i.e. $\omega\gg d$ and in particular $\{\omega_n,\omega_{sn},\omega_{bn},\Omega\}\gg\{d_n,d_{en},d_{in}\}$. This assumption makes it possible to calculate the real part of

Eq. (17) at zero order relative to d and the imaginary part of this same equation at first order relative to d:

$$\Psi_n\omega_n^4 - \Gamma_n\Omega\omega_n^3 - (\omega_{sn}^2 + \Pi_n\omega_{bn}^2)\omega_n^2 + \Gamma_n\Omega\omega_{bn}^2\omega_n + \omega_{bn}^2\omega_{sn}^2 = \mathcal{O}(\omega^3 d) \approx 0, \tag{20}$$

$$(d_{in} + \Pi_n d_{en} - d_n 4\Psi_n)\omega_n^3 - (d_{in} + d_{en}\Gamma_n - 3A_n\Gamma_n)\Omega\omega_n^2 - (d_{en}\omega_{sn}^2 + d_{in}\omega_{bn}^2 - 2d_n\omega_{sn}^2 + \Pi_n\omega_{bn}^2)\omega_n + d_{in}\omega_{bn}^2\Omega - d_n\Gamma_n\omega_{bn}^2\Omega = \mathcal{O}(\omega^2 d^2) \approx 0. \tag{21}$$

Eq. (20) has the advantage of being independent of d_n and gives the four eigenvalues of the system directly as a function of the spin speed. From this equation, it is then possible to directly obtain an analytical expression for the critical speeds (noted ω_{cn}): when the shaft reaches a forward critical speed, the spin speed is equal to ω_{cn}, and Eq. (20) therefore becomes

$$\Delta_{n1}\omega_n^4 - (\omega_{sn}^2 + \Delta_{n2}\omega_{bn}^2)\omega_n^2 + \omega_{bn}^2\omega_{sn}^2 = 0 \quad \text{with } \Delta_{n1} = \Psi_n - \Gamma_n,\ \ \Delta_{n2} = \Pi_n - \Gamma_n. \tag{22}$$

In the case of the backward critical speeds, the spin speed is equal to $-\omega_{cn}$, and Eq. (20) therefore becomes:

$$\Delta_{n3}\omega_n^4 - (\omega_{sn}^2 + \Delta_{n4}\omega_{bn}^2)\omega_n^2 + \omega_{bn}^2\omega_{sn}^2 = 0 \quad \text{with } \Delta_{n3} = \Psi_n + \Gamma_n,\ \ \Delta_{n4} = \Pi_n + \Gamma_n. \tag{23}$$

Hence, the four critical speeds of the harmonic n are:

$$\omega_{cnF\pm} = \left[\frac{\omega_{sn}^2 + \Delta_{n2}\omega_{bn}^2 \pm \sqrt{\omega_{sn}^4 + 2(\Delta_{n2} - 2\Delta_{n1})\omega_{sn}^2\omega_{bn}^2 + \Delta_{n2}^2\omega_{bn}^4}}{2\Delta_{n1}}\right]^{\frac{1}{2}}, \tag{24}$$

$$\omega_{cnB\pm} = -\left[\frac{\omega_{sn}^2 + \Delta_{n4}\omega_{bn}^2 \pm \sqrt{\omega_{sn}^4 + 2(\Delta_{n4} - 2\Delta_{n3})\omega_{sn}^2\omega_{bn}^2 + \Delta_{n4}^2\omega_{bn}^4}}{2\Delta_{n3}}\right]^{\frac{1}{2}}, \tag{25}$$

where $\pm$ stands for the two equations with positive sign and negative sign, written in contracted form. The angular frequencies ω_{cnB-} and ω_{cnB+} are the backward critical speeds, and the other two, ω_{cnF-} and ω_{cnF+}, are the forward critical speeds.

Eq. (21) relates directly the modal damping d_n to the angular frequencies ω_n:

$$d_n(\Omega) = d_{in}\frac{\omega_n^3\left(1 + \dfrac{d_{en}}{d_{in}}\Pi_n\right) - \left(\omega_{bn}^2 + \dfrac{d_{en}}{d_{in}}\omega_{sn}^2\right)\omega_n + \left(\omega_{bn}^2 - \omega_n^2\left(1 + \dfrac{d_{en}}{d_{in}}\Gamma_n\right)\right)\Omega}{2\omega_n(2\Psi_n\omega_n^2 - \omega_{sn}^2 - \Pi_n\omega_{bn}^2) + \Gamma_n(\omega_{bn}^2 - 3\omega_n^2)\Omega}. \tag{26}$$

This equation therefore gives the stability of the system. An analytical solution for this expression can be obtained if there exists an analytical solution for ω_n. Let us assume the gyroscopic effects to be insignificant in comparison with the inertia effects, i.e. $\Gamma_n \approx 0$. This assumption is particularly valid in the case of the very first modes and that of thin tubes [13]. Eq. (20) therefore becomes a biquadratic equation which is independent of the spin speed. These directly gives the following four analytical solutions ω_{np0}:

$$\omega_{nF+0} = -\omega_{nB+0} = \left[\frac{\omega_{sn}^2 + \Pi_n\omega_{bn}^2 + \sqrt{\omega_{sn}^4 + 2(\Pi_n - 2\Psi_n)\omega_{sn}^2\omega_{bn}^2 + \Pi_n^2\omega_{bn}^4}}{2\Psi_n}\right]^{\frac{1}{2}}, \tag{27}$$

$$\omega_{nF-0} = -\omega_{nB-0} = \left[\frac{\omega_{sn}^2 + \Pi_n\omega_{bn}^2 - \sqrt{\omega_{sn}^4 + 2(\Pi_n - 2\Psi_n)\omega_{sn}^2\omega_{bn}^2 + \Pi_n^2\omega_{bn}^4}}{2\Psi_n}\right]^{\frac{1}{2}}. \tag{28}$$

The angular frequencies ω_{nB-0} and ω_{nB+0} are the backward whirl speeds, and the other two, ω_{nF-0} and ω_{nF+0}, are the forward whirl speeds. Due to the assumption that there exist only weak gyroscopic effects, these are independent of the spin speed. Analysis of Eqs. (27) and (28) gives the following relations

(for proof, see Appendix A):

$$\omega_{nB-0}^2 = \omega_{nF-0}^2 < \omega_{bn}^2 < \omega_{nB+0}^2 = \omega_{nF+0}^2, \tag{29}$$

$$\omega_{nB-0}^2 = \omega_{nF-0}^2 < \frac{\omega_{sn}^2}{\Pi_n} < \omega_{nB+0}^2 = \omega_{nF+0}^2. \tag{30}$$

These inequalities show that the natural frequencies resulting from coupling effects between rigid-body modes and flexural modes frame the uncoupled ones.

With the previous assumption that are the gyroscopic effects negligible, the modal damping of the npth mode ($n \in \mathbb{N}^*$ and $p \in \{B-, B+, F-, F+\}$) is expressed according to Eq. (26) as follows:

$$d_{np0}(\Omega) = d_{in} \frac{\omega_{np0}^3 \left(1 + \dfrac{d_{en}}{d_{in}} \Pi_n\right) - \left(\omega_{bn}^2 + \dfrac{d_{en}}{d_{in}} \omega_{sn}^2\right) \omega_{np0} + (\omega_{bn}^2 - \omega_{np0}^2)\Omega}{2\omega_{np0}(2\Psi_n \omega_{np0}^2 - \omega_{sn}^2 - \Pi_n \omega_{bn}^2)}. \tag{31}$$

Classically, the sign of this equation for $n \in \{1, \ldots, N\}$ and $p \in \{B-, B+, F-, F+\}$ gives the stability of the rotor system. When the modal damping d_{np} becomes negative, the shaft is unstable. To study the last equation, it is necessary first to express the external and internal damping.

2.1. External damping

In configuration 1, the external modal damping d_{en} is assumed to be viscous and to be equal to $c_e(4 + 2(-1)^n)/m_e$ according to Eq. (14) since in this case $m_s = 0$.

In configuration 2, the external modal damping d_{en} is assumed to be hysteretic. To introduce hysteretic damping, it is convenient to use an equivalent viscous damping constant c_{eq} as follows:

$$c_{\text{eq}} = \frac{\eta k}{|\omega|}, \tag{32}$$

where η is the loss factor, k is the stiffness and ω is the excitation frequency. Problems arise when the mechanical system is excited by several frequencies, as in the case of a rotor. The previously used substitution procedure is not very suitable here, since ω can take several values simultaneously. Wettergren [5] has analysed this problem and shown both theoretically and experimentally that the critical speeds can be handled separately. External damping of the npth mode can therefore be expressed as $\eta_e k_e / |\omega_{np}(\Omega)|$. Assuming the gyroscopic effects to be negligible, the frequency ω_{np} is approximated by ω_{np0} (Eqs. (27), (28)) and the external modal damping can therefore be expressed as follows:

$$d_{en}(\Omega) = \frac{\eta_e \omega_{bn}^2}{|\omega_{np0}|}. \tag{33}$$

Finally, with the above assumptions, the external modal damping is a constant in both configurations and therefore does not depend on the spin speed.

2.2. Shaft with internal viscous damping

If the shaft damping is assumed to be viscous, the internal modal damping d_{in} will be constant and can be expressed according to Eq. (14) as $c_i/\rho S$. The external and internal damping therefore do not depend on the spin speed. Assuming the gyroscopic effects to be negligible, the sign of Eq. (31) can be studied directly. Eqs. (29) and (30) show that (for details, see Appendix B): d_{nB-0} and d_{nB+0} are positive at null speed and are strictly increasing quantities depending on the speed; d_{nF-0} and d_{nF+0} are positive at null speed and are also strictly decreasing quantities depending on the speed. It can thus be concluded that only forward modes $nF-$ and $nF+$ can be unstable. The instability threshold can be obtained by solving $d_{nF-0} < 0$ and $d_{nF+0} < 0$.

This shows that the shaft will be unstable if:

$$\Omega > \omega_{nF\pm0}\left(1+\frac{d_{en}}{d_{in}}\frac{\Pi_n\omega_{nF\pm0}^2-\omega_{sn}^2}{\omega_{nF\pm0}^2-\omega_{bn}^2}\right)=\Omega_{\text{ths.visc}.nF\pm}. \tag{34}$$

With these assumptions, the instability threshold have a similar form to that of the well-known equation obtained by Smith [15] for the Jeffcott rotor: $\Omega_{\text{ths.visc}}=\omega_s(1+(c_e/c_i))$, where ω_s is the forward critical speed (see also Refs. [7,16]), i.e. the internal damping has a destabilizing effect on the forward whirl modes, the external damping always has a stabilizing effect, while the backward whirl modes are always stable. In addition, the instabilities always take place in the supercritical field, since $(\Pi_n\omega_{nF\pm0}^2-\omega_{sn}^2)/(\omega_{nF\pm0}^2-\omega_{bn}^2)>0$ according to Eqs. (29) and (30).

2.3. Shaft with internal hysteretic damping

Shaft damping is now assumed to be hysteretic. Damping of this kind is introduced via the previous equivalence (32). Internal damping has to be considered in the rotating frame of reference. The excitation frequency therefore corresponds to $|\omega_{np}(\Omega)-\Omega|$. In this case, equivalent internal damping can be written in the following form:

$$c_{\text{eq}}=\frac{\eta_i k_{sn}}{|\omega_{np}(\Omega)-\Omega|l}. \tag{35}$$

Assuming the gyroscopic effects to be negligible, i.e. $\omega_{np}(\Omega)=\omega_{np0}$ and noting that $\omega_{sn}^2=k_{sn}/m_s$, $d_{in}=c_{\text{eq}}/\rho S$ according to Eq. (14) and $m_s=\rho Sl$, the internal modal damping can be written in the following form:

$$d_{in}(\Omega)=\frac{\eta_i\omega_{sn}^2}{|\omega_{np0}-\Omega|}. \tag{36}$$

Assuming $\Omega\geqslant0$, the absolute value can be removed:

$$d_{in}(\Omega)=\frac{\eta_i\omega_{sn}^2}{\Omega-\omega_{np0}}\quad \text{for } p\in\{B-,B+\} \text{ or } p\in\{F-,F+\} \text{ and } \Omega>\omega_{nF\pm0}, \tag{37}$$

$$d_{in}(\Omega)=\frac{\eta_i\omega_{sn}^2}{\omega_{np0}-\Omega}\quad \text{for } p\in\{F-,F+\} \text{ and } \Omega<\omega_{nF\pm0}. \tag{38}$$

These previous equations can be introduced into Eq. (31). In the backward modes, the internal modal damping is therefore

$$d_{nB\pm0}(\Omega)=\frac{-\eta_i\omega_{sn}^2(\omega_{nB\pm0}^2-\omega_{bn}^2)+d_{en}\omega_{nB\pm0}(\Pi_n\omega_{nB\pm0}^2-\omega_{sn}^2)}{2(2\Psi_n\omega_{nB\pm0}^2-\omega_{sn}^2-\Pi_n\omega_{bn}^2)\omega_{nB\pm0}}, \tag{39}$$

in the forward modes in the subcritical range (noted sub), it is

$$d_{nF\pm0.sub}(\Omega)=\frac{\eta_i\omega_{sn}^2(\omega_{nF\pm0}^2-\omega_{bn}^2)+d_{en}\omega_{nF\pm0}(\Pi_n\omega_{nF\pm0}^2-\omega_{sn}^2)}{2(2\Psi_n\omega_{nF\pm0}^2-\omega_{sn}^2-\Pi_n\omega_{bn}^2)\omega_{nF\pm0}} \tag{40}$$

and in the forward modes in the supercritical range (noted sup), it is

$$d_{nF\pm0.sup}(\Omega)=\frac{-\eta_i\omega_{sn}^2(\omega_{nF\pm0}^2-\omega_{bn}^2)+d_{en}\omega_{nF\pm0}(\Pi_n\omega_{nF\pm0}^2-\omega_{sn}^2)}{2(2\Psi_n\omega_{nF\pm0}^2-\omega_{sn}^2-\Pi_n\omega_{bn}^2)\omega_{nF\pm0}}. \tag{41}$$

As shown by Eqs. (39)–(41), internal hysteretic damping yields a constant modal damping, contrary to what occurs in the case of viscous damping. Note that the only difference between Eqs. (40) and (41) is the sign of the internal damping. If the internal damping is too large, the modal damping $d_{nF\pm0.sup}$ can be negative and the system will tend to be unstable. From Eqs. (39)–(41), the following conclusion can be reached, as in the case of the internal viscous damping (see Appendix C): backward whirl modes are always stable and forward whirl modes can be unstable only in the supercritical range. This important conclusion confirms the role of

hysteretic damping in rotors described by Genta [6,7]. Hysteretic damping has sometimes been poorly understood, since it has been thought to result in unstable forward whirl modes even at null speeds. This is physically impossible, because damping instabilities are due to forward modes which rotate in the negative direction in the rotational frame of reference, i.e. when $\omega_{nF\pm} - \Omega < 0$. This is possible only in the supercritical range, whatever the damping model used (viscous, hysteretic or other). In this case only, the dissipation force will tend to push the forward mode towards the outside, resulting in instability.

Instability of the forward mode develops when $d_{nF\pm 0.sup} < 0$. Assuming the gyroscopic effects to be negligible, the instability criterion can be expressed in the case of both configurations 1 and 2 as follows (as shown in Appendix C):

$$d_{en}\omega_{nF+0}(\Pi_n\omega_{nF+0}^2 - \omega_{sn}^2) - \eta_i\omega_{sn}^2(\omega_{nF+0}^2 - \omega_{bn}^2)\begin{cases} <0 & \Longrightarrow \quad \Omega_{\text{ths.hyst.}nF+} = \omega_{nF+0}, \\ \geqslant 0 & \Longrightarrow \quad \text{stable} \end{cases} \tag{42}$$

and

$$d_{en}\omega_{nF-0}(\Pi_n\omega_{nF-0}^2 - \omega_{sn}^2) - \eta_i\omega_{sn}^2(\omega_{nF-0}^2 - \omega_{bn}^2)\begin{cases} >0 & \Longrightarrow \quad \Omega_{\text{ths.hyst.}nF-} = \omega_{nF-0}, \\ \leqslant 0 & \Longrightarrow \quad \text{stable}, \end{cases} \tag{43}$$

these can be expressed in the case of configuration 2 as

$$\eta_e k_e \Phi_n(\Pi_n\omega_{nF+0}^2 - \omega_{sn}^2) - \eta_i k_{sn}(\omega_{nF+0}^2 - \omega_{bn}^2)\begin{cases} <0 & \Longrightarrow \quad \Omega_{\text{ths.hyst.}nF+} = \omega_{nF+0}, \\ \geqslant 0 & \Longrightarrow \quad \text{stable} \end{cases} \tag{44}$$

and

$$\eta_e k_e \Phi_n(\Pi_n\omega_{nF-0}^2 - \omega_{sn}^2) - \eta_i k_{sn}(\omega_{nF-0}^2 - \omega_{bn}^2)\begin{cases} >0 & \Longrightarrow \quad \Omega_{\text{ths.hyst.}nF-} = \omega_{nF-0}, \\ \leqslant 0 & \Longrightarrow \quad \text{stable.} \end{cases} \tag{45}$$

In the case of configuration 2, this instability criterion has a similar form to that obtained by Genta [7] for the Jeffcott rotor with internal and external hysteretic damping: "$\eta_e k_e - \eta_i k_s < 0 \Longrightarrow$ *forward whirl is unstable throughout the supercritical domain*" (where k_s is the stiffness of the shaft).

Eqs. (42)–(45) show that the stability depends greatly on the values of $\eta_i k_s$ and $\eta_e k_e$, but less commonly, that it also depends on the differences $\omega_{nF\pm0}^2 - \omega_{bn}^2$ and $\Pi_n\omega_{nF\pm0}^2 - \omega_{sn}^2$. When ω_{sn} and ω_{bn} are very different, for example, assuming that $\omega_{sn}^2 \gg \omega_{bn}^2$, the coupling effect between rigid-body modes and flexural modes will be weak, i.e. $\omega_{nF+0}^2 \to \omega_{sn}^2/\Psi_n$ according to Eq. (27) and $\omega_{nF-0}^2 \to \Pi_n\omega_{bn}^2/\Psi_n$ according to Eq. (28), where Π_n and Ψ_n are approximately equal to 1 when n is small. Consequently, when values of $\eta_i k_s$ and $\eta_e k_e \Phi_n$ are reasonably realistic, the external damping part of the $nF-$ mode will be large (and negative) according to Eq. (45), whereas the internal damping part will be small, and it can therefore be concluded that this mode will tend to be stable. On the other hand, when this analysis is carried out on the $nF+$ mode according to Eq. (44), the results show that this mode will tend to be unstable. The stability therefore depends on the level of hysteretic damping and likewise on the coupling between rigid-body modes and flexural modes, i.e. on the similarity between the two mode frequencies.

Lastly, it should be noted, as in the case of viscous damping, that when no external damping is present, i.e. $\eta_e = 0$, the supercritical range will always be unstable.

3. Numerical examples and discussion

3.1. Case study 1: shaft with viscous internal damping mounted on undamped and damped isotropic flexible bearings

Few studies have dealt so far with shafts without disks, taking the internal and external damping into account. In order to confirm the validity of the above analysis and criteria, we first studied the case of a continuous shaft with undamped and damped flexible isotropic bearings under viscous internal damping conditions. This example has been studied by several authors [17–19] with various finite element models. Zorzi

and Nelson [17] have studied a Euler–Bernoulli beam finite element model, for instance, while Özgüven and Özkan [18] have introduced the shear parameter $a = 12EI/\kappa GSl^2$ into the previous finite elements, and Ku [19] have developed a Timoshenko beam finite element model. All these models take the effects of translational and rotatory inertia, the gyroscopic moments and the internal viscous damping into account.

The shaft and the bearings have the following physical parameters [17–19]:

$$E = 2.08 \times 10^{11}\,\text{Pa}, \quad \rho = 7830\,\text{kg m}^{-3}, \quad l = 1.27\,\text{m}, \quad r = 0.0508\,\text{m},$$

$$m_e = 0\,\text{kg}, \quad k_e = 1.7512 \times 10^{7}\,\text{N m}^{-1}, \quad c_e = 1.7512 \times 10^{3}\,\text{N s m}^{-1}, \quad \mu_i = 0.0002\,\text{s}$$

where μ_i is a viscous damping equal to $c_i l/k_n$ with our notations. The modal damping is therefore $d_{in} = \mu_i \omega_{sn}^2$. The computation is carried out with $n = 2$. From Eq. (14), the characteristics of the uncoupled system are:

$$\omega_{b1} = 659\,\text{rad s}^{-1}, \quad \omega_{b2} = 1142\,\text{rad s}^{-1}, \quad \omega_{s1} = 801\,\text{rad s}^{-1} \quad \text{and} \quad \omega_{s2} = 3204\,\text{rad s}^{-1}.$$

In the present study, the natural whirl speeds and the logarithmic decrement, defined as $\delta = 2\pi d/|\omega|$, can be computed using three methods. The first method consists in solving the characteristic equation (17) using numerical methods. The second method corresponds to finding the numerical solutions of Eqs. (20) and (21), which take the gyroscopic effects into account but involve the assumption that $\omega \gg d$. The third method consist in calculating the approximate solutions (27), (28) and (31), in which the gyroscopic effects is assumed negligible and $\omega \gg d$.

The Campbell diagram resulting from the solutions of Eq. (17) is presented in Fig. 3(a) for the shaft without external damping and in Fig. 3(b) for the shaft with external damping. The logarithmic decrement and the results obtained by Ku [19] are also given in these figures. The logarithmic decrement curves obtained using the three methods mentioned above are presented in Fig. 4(a) in the case of the shaft without any external damping and in Fig. 4(b) in that of the shaft with external damping. Lastly, Tables 1 and 2 present the whirl speeds and logarithmic decrements obtained with the same three methods at a spin speed $\Omega = 4000\,\text{rev/min}$ without any external damping, and these are compared with data available in the literature [17–19].

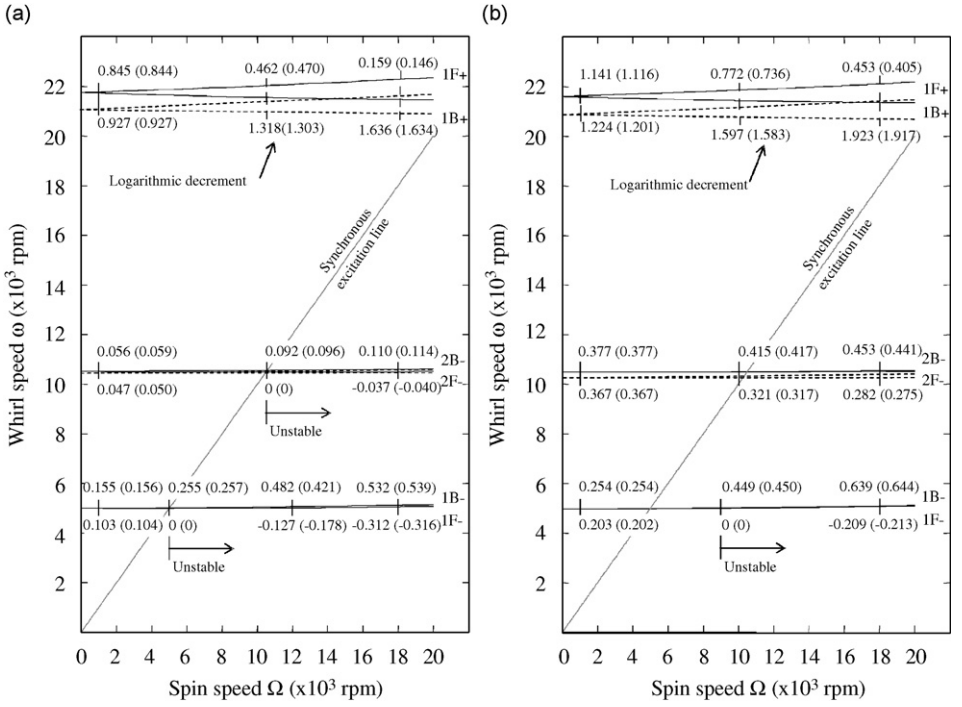

Fig. 3. Campbell diagram and logarithmic decrement of a shaft supported on undamped isotropic bearings (a) and damped isotropic bearings (b) with viscous damping $\mu_i = 0.0002\,\text{s}$ in the case of a Euler–Bernoulli beam model (— and δ from Eq. (17)) and in the case of a Timoshenko beam finite element model (- - - and (δ) from Ku [19]).

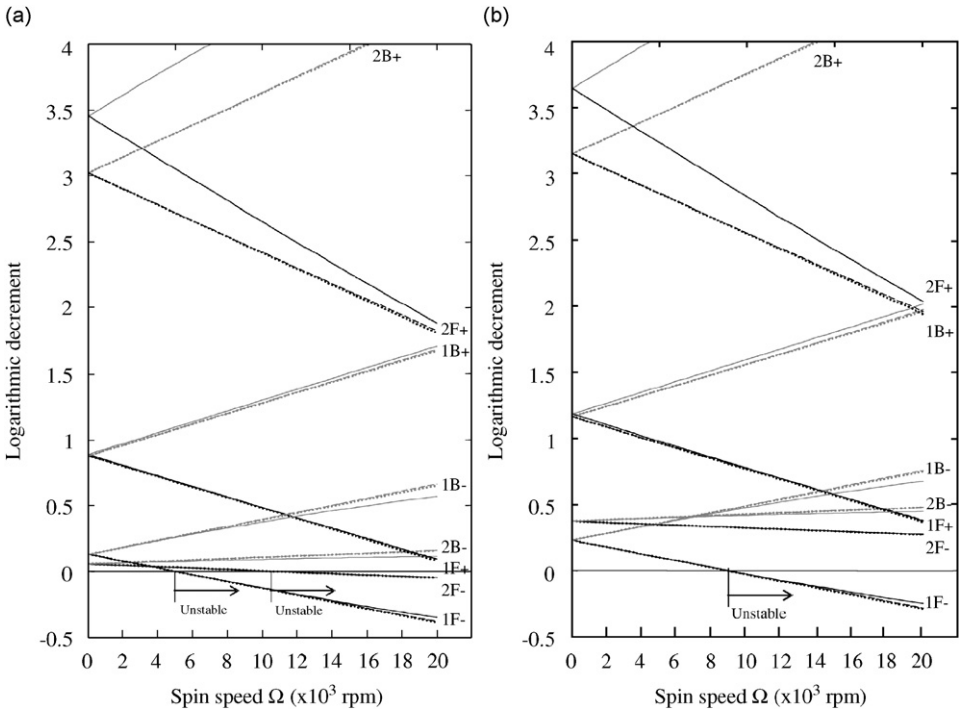

Fig. 4. Logarithmic decrement of a shaft supported on undamped isotropic bearings (a) and damped isotropic bearings (b) with viscous damping $\mu_i = 0.0002\,\mathrm{s}$ (— Eq. (17); – – Eqs. (20), (21); ⋯ Eq. (31)).

Table 1
Whirl speed ω (rad s^{-1}) of a shaft supported on undamped isotropic bearings with viscous damping $\mu_i = 0.0002\,\mathrm{s}$ at a spin speed $\Omega = 4000\,\mathrm{rev/min}$ using various models

Mode	Present work			Ref. [17]	Ref. [18]	Ref. [19]
	Eqs. (27), (28)	Eq. (20)	Eq. (17)			
$1F-$	521	522	522	521	520	521
$1B-$	521	521	523	523	522	522
$1F+$	2303	2311	2287	2231	2223	2217
$1B+$	2303	2294	2268	2214	2206	2201
$2F-$	1098	1098	1099	1097	1096	1095
$2B-$	1098	1098	1101	1097	1095	1095
$2F+$	5217	5233	4588	4492	4447	4413
$2B+$	5217	5201	4552	4454	4412	4379

In the case of the shaft without any external damping, the results given in Fig. 3(a) and Table 1 show excellent agreement with previously published data in the case of whirl speeds denoted −. The difference is more significant in the case of forward whirl speeds denoted +. Comparisons between results obtained using Eq. (17) and those obtained by Zorzi and Nelson show that whirl speeds $1F+$ and $1B+$ differ by approximately 2.4% and whirl speeds $2F+$ and $2B+$ by approximately 2.2%. In the case of the shaft with external damping (Fig. 3(b)), the differences are similar but whirl speeds $2F-$ and $2B-$ also differ by approximately 2.2%. More significant differences are observed with results presented by Özgüven et al. and Ku (between 3% and 4%) and these are probably due to shear effects, whereas these effects are neglected in the present study, as in the finite elements study by Zorzi et al.

As shown in Table 1, all the methods yielded the same results in the case of whirl speeds denoted −, which are almost independent of the spin speed. These modes correspond mainly to the rigid-body modes, which are

Table 2
Logarithmic decrement δ of a shaft supported on undamped isotropic bearings with viscous damping $\mu_i = 0.0002\,\mathrm{s}$ at a spin speed $\Omega = 4000\,\mathrm{rev/min}$ using various models

Mode	Present work			Ref. [17]	Ref. [18]	Ref. [19]
	Eqs. (27), (28), (31)	Eqs. (20), (21)	Eq. (17)			
$1F-$	0.0254	0.0254	0.0254	0.0253	0.0252	0.0252
$1B-$	0.2330	0.2338	0.2303	0.2309	0.2321	0.2325
$1F+$	0.7169	0.7178	0.7234	0.7250	0.7830	0.7187
$1B+$	1.0357	1.0357	1.0502	1.0590	1.0540	1.0528
$2F-$	0.0335	0.0334	0.0329	0.0331	0.0341	0.0347
$2B-$	0.0748	0.0750	0.0691	0.0687	0.0709	0.0723
$2F+$	2.7781	2.7990	3.1325	3.0480	2.9810	2.9409
$2B+$	3.2632	3.2638	3.7690	3.6810	3.6070	3.5634

not very sensitive to gyroscopic effects. On the other hand, significant differences are found to exist between the three methods in the case of whirl speeds denoted +, especially in modes $2F+$ and $2B+$. The difference between the solution of Eqs. (20), (21) and the solution of Eq. (17) is due to the weak damping assumption ($\omega \gg d$), and this assumption is not true here ($\delta \gtrsim 3$ i.e. $d \gtrsim |\omega|/2$, as shown in Table 2). In this case, the damping $c_i l$ is equal to $2.064 \times 10^4\,\mathrm{N\,s\,m^{-1}}$ with $n = 1$ and $3.312 \times 10^5\,\mathrm{N\,s\,m^{-1}}$ with $n = 2$. These values mean that the internal damping $\mu_i = 0.0002\,\mathrm{s}$ is extremely high, and not very realistic or of purely academic interest. In addition, the whirl speeds given by Eqs. (20), (21) and Eqs. (27), (28) show a good agreement (Table 1). This confirms the assumption that the gyroscopic effects are negligible in these first modes. More significant differences are likely to occur at higher spin speeds, since Eqs. (27), (28) are constant. However, it can be concluded that analytically calculated whirl speeds (Eqs.(27), (28)) are accurate.

The logarithmic decrements presented in Fig. 3 and Table 2 show good agreement. Comparison between the results given by Eq. (17) and those published by Zorzi et al. (Table 2) show the existence of differences of less than 3% in the modes $2F+$ and $2B+$ and less than 1% in the other modes. Moreover, based on Fig. 4 and Table 2, all the values obtained here are very similar in the modes $1F-$ to $2B-$. On the other hand, the logarithmic decrements obtained in modes $2F+$ and $2B+$ differ significantly. These differences are mainly due to the difference in the whirl speed ω, because the errors on the modal damping $d = \delta|\omega|/2\pi$ amounted to less than 1%. In addition, the logarithmic decrements obtained from Eqs. (20), (21) and Eqs. (27), (28), (31) show good agreement (dashed and dotted lines in Fig. 4). As with the whirl speeds, this confirms the assumption that the gyroscopic effects are negligible. Lastly, it can be seen by comparing Figs. 4(a) and (b) that including the external damping in the model increases all the logarithmic decrements, which tend to shift the instability threshold to a higher spin speed.

As far as stability is concerned, the present results are in good agreement with previously published data. When there is no external damping, instability occurs only in the forward modes and the instability threshold begins at the critical speed (Figs. 3(a) and 4(a)). Under external damping conditions, the instability threshold is shifted to a higher spin speed (Fig. 3(b)). The instability threshold of the mode $1F-$ occurs at a spin speed of 8889 rev/min according to Eq. (17), 8862 rev/min according to Eqs. (20), (21) and 8804 rev/min according to the analytical criterion (Eq. (34)). Ku obtained an instability threshold in the same mode at a spin speed of 8800 rev/min and Zorzi et al. obtained a value of 9200 rev/min. Comparisons between these results show that the analytical instability criterion gives accurate results.

3.2. Case study 2: shaft with hysteretic internal damping with undamped and damped isotropic flexible bearings

The same shaft is studied here as in case 1, but the internal viscous damping is replaced by hysteretic damping. Previous authors [17–19] have studied this case with the above physical parameters and a loss factor η_i equal to 0.0002. This value is extremely low although Zorzi et al. and Ku [17,19] reported that this hysteretic damping destabilized all the forward modes at any spin speed, even at null speed. As previously established, this is physically impossible [6].

A more realistic loss factor value, in the case of steel for example, ranges between 0.002 and 0.004. These values are low and they can be higher with other materials such as carbon/epoxy laminate materials because of the epoxy resin (depending of course on the stacking sequence). To obtain more conspicuous effects of the internal damping on the simulations presented here, it was therefore proposed to use a loss factor $\eta_i = 0.04$.

In this example, as in the viscous case, the whirl speeds and logarithmic decrements can be computed using three methods. The first method consists in solving the characteristic equation (17) numerically. However, this computation is more complex than in the previous case because the internal modal damping ((37), (38)) requires knowing the whirl speeds, which means using an iterative process. In addition, the hysteretic damping model gives rise to convergence problems at the critical speeds: at these speeds, the internal modal damping ((37), (38)) tends to infinity because the whirl speed tends to zero in the rotating frame of reference. Therefore, the computation of Eq. (17) is first carried out without any internal damping, in order to obtain an approximation of the whirl speed values, and several iterations are then carried out with the corresponding internal damping values. Divergence occurs very quickly when a spin speed approaches a whirl speed. The second method corresponds to finding the numerical solutions of Eqs. (20), (21), which involve the assumption that $\omega \gg d$. This method is a direct method because Eq. (20) does not include a damping term. The third method consists in calculating the approximate solutions and instability criteria (27), (28), (39)–(41), in which gyroscopic effects are assumed to be negligible and $\omega \gg d$.

The Campbell diagram and logarithmic decrement resulting from solution of Eq. (17) are presented in Fig. 5(a) for the shaft without external damping and in Fig. 5(b) for the shaft with external damping. The logarithmic decrement curves obtained using the three methods described here are presented in Fig. 6(a) for the shaft without external damping and in Fig. 6(b) for the shaft with external damping. Lastly, Table 3 gives the whirl speeds and logarithmic decrements obtained using the three methods at a spin speed $\Omega = 4000\,\mathrm{rev/min}$, without any external damping.

Comparisons between Figs. 5(a) and (b) show that whirl speeds are not affected by incorporating external damping. The good agreement observed between the solutions of Eq. (20) and Eq. (17) in Table 3 confirms

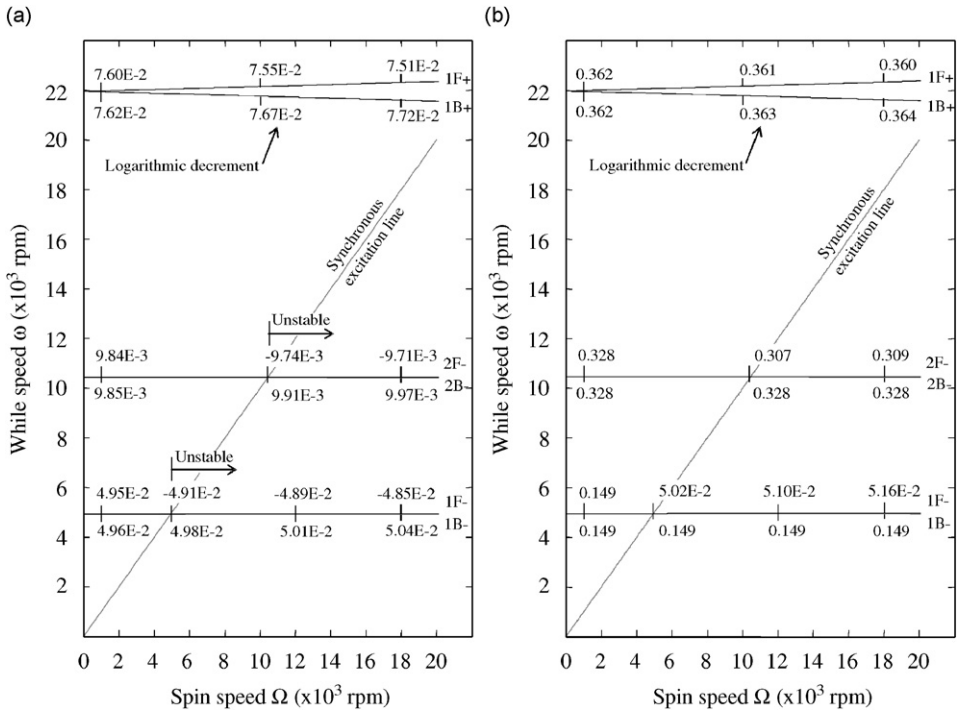

Fig. 5. Campbell diagram of a shaft supported on undamped isotropic bearings (a) and damped isotropic bearings (b) with hysteretic damping $\eta_i = 0.04$ (— Eq. (17) without internal damping; δ corresponding to Eq. (17) with internal damping).

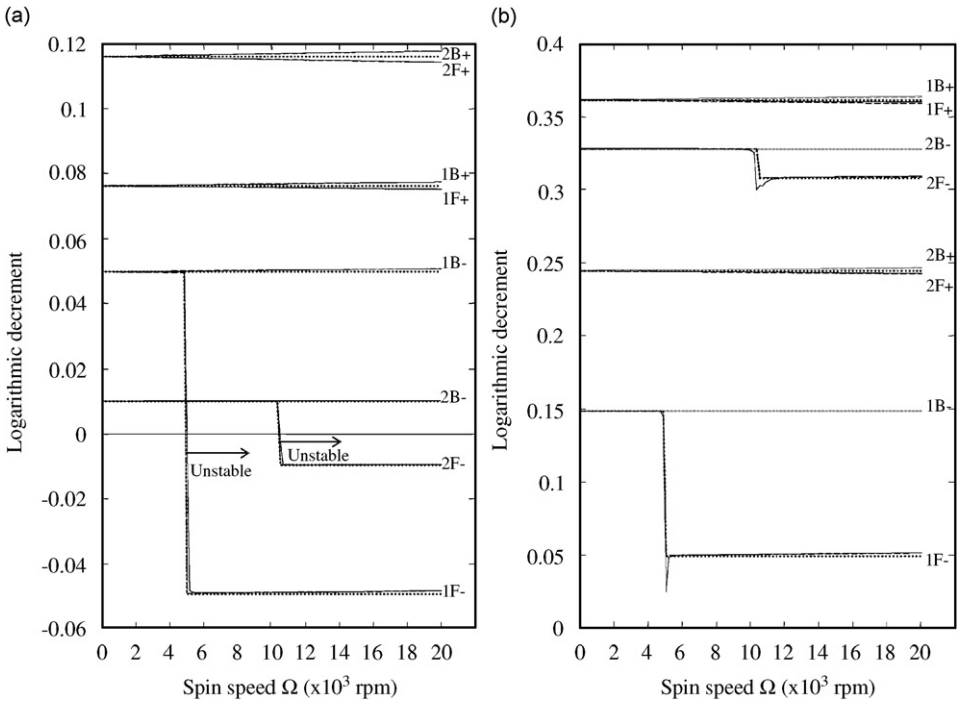

Fig. 6. Logarithmic decrement of a shaft supported on undamped isotropic bearings (a) and damped isotropic bearings (b) with hysteretic damping $\eta_i = 0.04$ (— Eq. (17); – – Eqs. (20), (21); ··· Eqs. (39)–(41)).

Table 3
Whirl speed and logarithmic decrement of a shaft supported on undamped isotropic bearings with hysteretic damping $\eta_i = 0.04$ at a spin speed $\Omega = 4000\,\mathrm{rev/min}$

Mode	ω (rad s^{-1})			$\delta(-)$		
	Eqs. (27), (28)	Eq. (20)	Eq. (17)	Eqs. (27), (28), (39)–(41)	Eqs. (20), (21)	Eq. (17)
$1F-$	498	498	498	0.0496	0.0494	0.0494
$1B-$	498	498	498	0.0496	0.0498	0.0497
$1F+$	2199	2207	2207	0.0761	0.0759	0.0759
$1B+$	2199	2191	2191	0.0761	0.0763	0.0763
$2F-$	1049	1049	1049	0.0099	0.0098	0.0098
$2B-$	1049	1049	1049	0.0099	0.0099	0.0099
$2F+$	4982	4997	4997	0.1158	0.1155	0.1155
$2B+$	4982	4966	4966	0.1158	0.1162	0.1162

this finding. The assumption that weak damping was involved is therefore true. The approximate solutions (27), (28), yield exactly the same results in the modes denoted − and very similar results in the modes denoted +, amounting to a difference of only about 0.3% at $\Omega = 4000\,\mathrm{rev/min}$. The assumption that weak gyroscopic effects were involved is therefore also true.

The logarithmic decrement curves in Figs. 6(a) and (b) are typical hysteretic damping curves. Without any external damping (Fig. 6(a)), the logarithmic decrement curves of the backward modes are positive and approximately constant, whereas those of the forward modes are positive and approximately constant until the corresponding critical speed is reached and they suddenly shift to a negative sign, which makes the system unstable. It can be noted that the logarithmic decrements obtained using all three methods proposed here give very similar results (Fig. 6 and Table 3). When external damping is present (Fig. 6(b)), the logarithmic

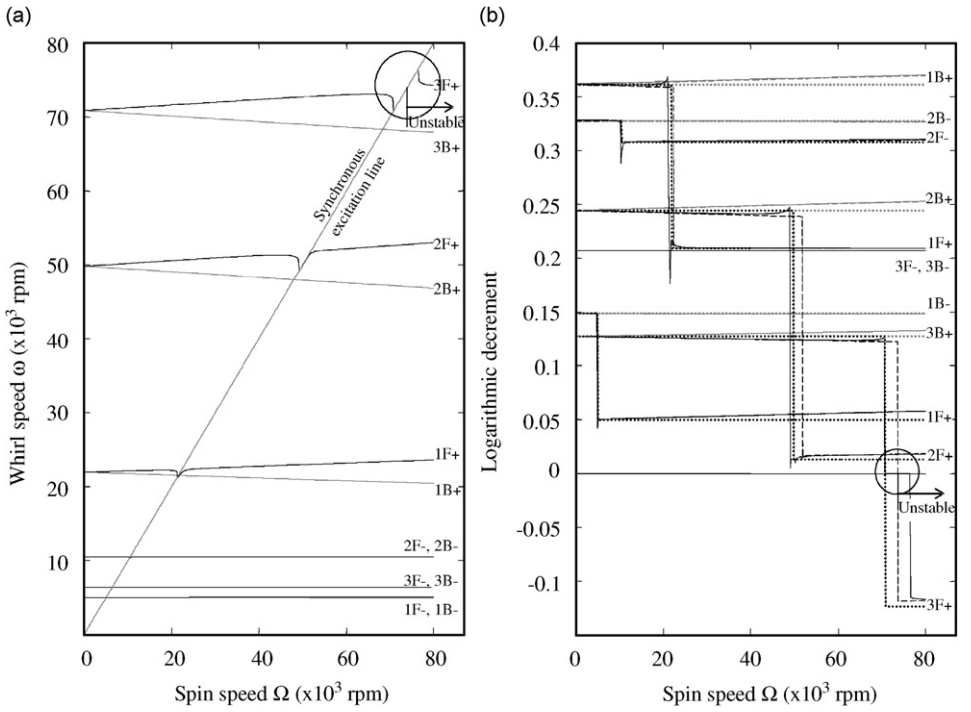

Fig. 7. Campbell diagram (a: — Eq. (17) with 100 iterations) and logarithmic decrement (b: — Eq. (17) with 100 iterations; – – Eqs. (20), (21); ⋯ Eqs. (39)–(41)) of a shaft supported on damped isotropic bearings with hysteretic damping $\eta_i = 0.04$. The overestimated internal damping close to the $3F+$ critical speed is magnified in the circles.

decrement curves are shifted upwards. In the speed range under consideration, the system is stable since all the logarithmic decrements are positive. Here again, the results obtained with the three methods are found to be in good agreement, except near the critical speeds, where divergence occured in the computation of Eq. (17) (solid lines in Fig. 6(b)).

The threshold speed was investigated at a spin speed greater than 20 000 rev/min under external damping conditions. The Campbell diagram and logarithmic decrement with $n = 3$ are given in Fig. 7. Whirl speeds and corresponding logarithmic decrements were obtained by solving Eq. (17) with the previously described iterative method. This computation was carried out by performing 100 iterations. Similar results were obtained when a larger number of iterations was performed. It can be seen from Fig. 7 that the results of the hysteretic damping model are not physically relevant at spin speed close to any forward critical speed. For example, when Ω is close to ω_{3F+} (in the zone surrounded by a circle in Fig. 7(a)), it can be written $d_{i3F+} \gg \{\omega_{3F+}, \omega_{s3F+}, \omega_{b3F+}, d_{e3F+}\}$ then Eq. (17) divided by d_{i3F+} at order 0 relatively to ω/d can be written as follows:

$$-\mathrm{i}\lambda_{3F+}^3 + \mathrm{i}\Omega\lambda_{3F+}^2 + \mathrm{i}\omega_{b3F+}^2\lambda_{3F+} - \mathrm{i}\Omega\omega_{b3F+}^2 = \mathcal{O}\left(\frac{\omega^4}{d}\right) + \mathrm{i}\mathcal{O}\left(\frac{\omega^4}{d}\right) \approx 0.$$

This equation has the obvious solution $\lambda_{3F+} = \Omega$, which means that $\omega_{3F+} = \Omega$ and $d_{3F+} = 0$. This result corresponds to the zones surrounded by the circles in Fig. 7, and was also obtained in Ref. [6] without any explanation being given by the author. However, one must to be careful about this result since hysteretic damping has no significance in the case of non-sinusoidal excitation and the excitation frequency tends here to 0. The results obtained in this zone are obviously different from those obtained with the other two methods, where weak damping was assumed to occur. However, the three methods including the instability criterion (Eq. (42)) give the threshold speeds corresponding to the $3F+$ critical speed i.e. at a spin speed $\Omega =$ 73 654 rev/min according to Eq. (24) and $\Omega =$ 73 681 rev/min according to Eq. (20). Finally, let us note that the instability threshold was found to be in the same mode with a ten-fold lower hysteretic internal damping

value, i.e. $\eta_i = 0.004$. This point confirms the fact that differences $\omega_{nF\pm0}^2 - \omega_{bn}^2$ and $\Pi_n\omega_{nF\pm0}^2 - \omega_{sn}^2$ decisively determine the occurence of instability (Eqs. (42) and (43)).

All these results show that the instability criterion gives accurate results for determining the instability threshold speed in the case of hysteretic internal damping.

3.3. Case study 3: shaft with infinitely rigid bearings mounted on viscoelastic supports

It is now proposed to compare configuration 1 (case studies 1 and 2) with configuration 2 (Fig. 2), i.e. isotropic damped flexible bearings with infinitely rigid bearings mounted on viscoelastic supports. These comparisons were carried out with previous data and additional data in the case of configuration 2:

$$m_e = 1\,\text{kg}, \quad k_e = 2 \times 10^6\,\text{N m}^{-1}, \quad \eta_e = 0.07.$$

On the other hand, the length of the shaft is now examined as a parameter. Let us note that the stiffness of the bearings in configuration 1 is ten times greater than the stiffness of the supports in configuration 2. This greatly affects the frequencies of the rigid-body modes.

With a given shaft length, the aim of this case study was to maximize the stability domain depending on the choice of these low cost supports (classical bearings or viscoelastically supported bearings). This study is quite simple, since the data on the bearings and supports are assumed to be independent of the shaft length. However, the kind of support is variably decisive, depending on the shaft length. Figs. 8(a) and (b) give whirl and threshold speed maps for configurations 1 and 2, respectively. The critical speeds were obtained from Eq. (24) and threshold speeds from Eq. (34) (with $\mu_i = 0.00002\,\text{s}$, i.e. μ_i is ten times lower than in case study 1) in the case of internal viscous damping and from Eqs. (42) and (43) (with $\eta_i = 0.04$) in that of hysteretic internal damping. In configuration 1, the efficiency zone of the bearing with external viscous damping is approximately in the $l \in [1, 2]\,\text{m}$ range. In the second configuration,

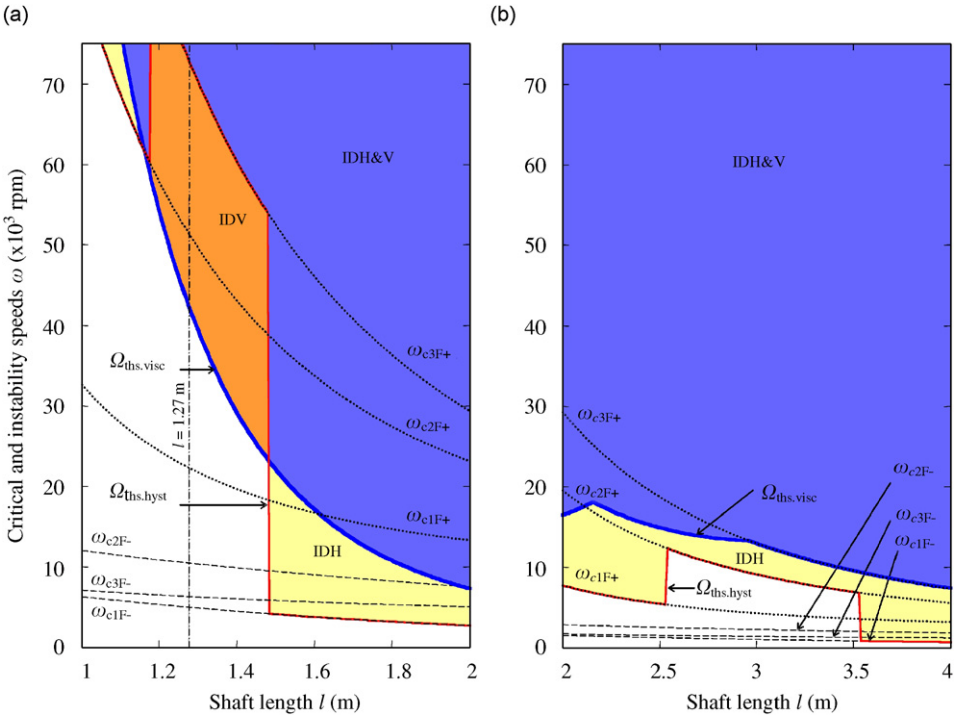

Fig. 8. Critical speeds and instability speeds versus shaft length given by configuration 1(a) and configuration 2(b) ($\cdots$ ω_{cnF+} and - - - ω_{cnF-}: Eq. (24); — $\Omega_{\text{ths.visc}}$: Eq. (34) with $\mu_i = 0.00002\,\text{s}$; — $\Omega_{\text{ths.hyst}}$: Eqs. (42), (43) with $\eta_i = 0.04$; IDV, IDH and IDH&V: instability domain for viscous model, for hysteretic model and for both models).

the efficiency zone of the viscoelastically supported bearing with external hysteretic damping is approximately in the $l \in [2,4]$ m range. In each figure, coloured areas correspond to the instability domains predicted either by the viscous internal damping model or by the internal damping hysteretic model or by both models.

The two figures show the stability zone located in the supercritical region with the two internal damping models. It can be seen here that in configuration 1 (Fig. 8(a)), the stability zone disappears at lengths greater than 1.48 m with hysteretic damping and tends to disappear at lengths greater than 2 m with viscous damping. In configuration 2, a stability zone located in the supercritical region is again visible in the case of both models. In particular, with the hysteretic model, this zone occurs between shaft lengths of 2.55 m and 3.56 m. These results show that viscoelastic supports are most efficient with very long shafts, which is particularly useful in the case of some applications, such as the long drivelines of helicopters and tiltrotors.

In these two figures, it is worth noting that both damping models can be seen to delimit very different zones, which shows the importance of determining the damping behaviour of the shaft material as well as other dissipative process occurring in the rotating frame of reference, such as friction between rotating parts.

4. Conclusion

The case of a rotating shaft with either internal damping and dissipative bearings or infinitely rigid bearings mounted on viscoelastic supports was investigated here using analytical methods. The aim of this paper was to compare the results obtained with the two usual models for internal damping: the viscous model and the hysteretic model. The latter model is classically held to simulate more closely the real damping behaviour of the materials usually used to produce rotating shafts. A Euler–Bernoulli beam model was proposed for the shaft, which neglects the shear effects but takes the effects of translational and rotatory inertia, gyroscopic moments, and internal viscous or hysteretic damping into account. Hysteretic damping was modelled by including an equivalent viscous damping term.

Assuming the damping to be weak and the gyroscopic effects to be negligible, this study focused mainly on the analytical critical speeds and instability criteria resulting from the addition of internal damping. When these assumptions did not give satisfactory results, the model was studied numerically. The form of the criteria obtained in both the viscous and hysteretic cases was in good agreement with those available in the literature on the Jeffcott rotor. These criteria clearly confirm the fact that internal damping instabilities can only exist in the forward whirl modes in the supercritical range, whatever the damping model used. Here we established in particular that the effects of the coupling between rigid-body modes introducing external damping and flexural modes are as important as the effects of the damping level, i.e. the stability greatly increases when a rigid-body frequency approaches a flexural frequency.

In the case of internal viscous damping, a comparative study showed that the results were in good agreement with those obtained with several finite element models in previous studies. Studies on internal hysteretic damping were carried out on the same example without making comparisons of this kind. The results obtained in this case were in line with those published on Jeffcott rotor. The third case study carried out here made it possible to determine the effects of viscoelastic supports on the stability in the supercritical range. This study showed that viscoelastic supports provide stability when classical bearings are less efficient, especially in the case of long shafts. Lastly, comparisons on the threshold speeds based on viscous and hysteretic damping models showed the existence of large differences. Although the two models are difficult to compare, since no real numerical correspondence exists between them, it is possible to conclude that the determination of instabilities of this kind is highly dependent on the damping model used. Therefore, to significantly improve the accuracy of threshold speed determinations, accurate material damping identification is first required. This means that more complex damping models such as frequency dependent damping models or combined viscous and hysteretic damping models are required. In this case, the model presented here would make it possible to efficiently carry out this analysis with numerical methods.

Appendix A. Proof of Eqs. (29) and (30)

If n is an odd number, based on Eq. (14), it can be written as:

$$0<\Phi_n=2\frac{m_s}{2m_e+m_s}\leqslant 2. \tag{A.1}$$

From previous equations, from several definitions in Eq. (18) and noting that $\Pi_n>1$, the following inequality can be obtained:

$$0<1-\frac{8}{n^2\pi^2\Pi_n}\leqslant\frac{\Psi_n}{\Pi_n}=1-\frac{4\Phi_n}{n^2\pi^2\Pi_n}<1. \tag{A.2}$$

Likewise, if n is an even number, it can be written

$$0<\Phi_n=6\frac{m_s}{6m_e+m_s}\leqslant 6, \tag{A.3}$$

therefore

$$0<1-\frac{24}{n^2\pi^2\Pi_n}\leqslant\frac{\Psi_n}{\Pi_n}=1-\frac{4\Phi_n}{n^2\pi^2\Pi_n}<1. \tag{A.4}$$

Finally, noting that $\Pi_n>0$, we obtain for all n:

$$0<\Psi_n<\Pi_n, \tag{A.5}$$

therefore

$$\Psi_n^2<\Pi_n\Psi_n \tag{A.6}$$

and consequently

$$4\Psi_n^2\omega_{bn}^4-4\Psi_n\Pi_n\omega_{bn}^4<0. \tag{A.7}$$

Adding the term $(\omega_{sn}^2+\Pi_n\omega_{bn}^2)^2-4\Psi_n\omega_{bn}^2\omega_{sn}^2$ to both sides of this inequality, the previous equation becomes:

$$\begin{aligned}&\omega_{sn}^4+2(\Pi_n-2\Psi_n)\omega_{sn}^2\omega_{bn}^2+\Pi_n^2\omega_{bn}^4+4\Psi_n^2\omega_{bn}^4-4\Psi_n\Pi_n\omega_{bn}^4\\&\quad<\omega_{sn}^4+2(\Pi_n-2\Psi_n)\omega_{sn}^2\omega_{bn}^2+\Pi_n^2\omega_{bn}^4.\end{aligned} \tag{A.8}$$

The left part of this inequality can be factorized as follows:

$$0<(\omega_{sn}^2+(\Pi_n-2\Psi_n)\omega_{bn}^2)^2<\omega_{sn}^4+2(\Pi_n-2\Psi_n)\omega_{sn}^2\omega_{bn}^2+\Pi_n^2\omega_{bn}^4. \tag{A.9}$$

The square root of the above expression yields two inequalities:

$$\begin{aligned}&\omega_{sn}^2+(\Pi_n-2\Psi_n)\omega_{bn}^2<\sqrt{\omega_{sn}^4+2(\Pi_n-2\Psi_n)\omega_{sn}^2\omega_{bn}^2+\Pi_n^2\omega_{bn}^4},\\&-\omega_{sn}^2-(\Pi_n-2\Psi_n)\omega_{bn}^2<\sqrt{\omega_{sn}^4+2(\Pi_n-2\Psi_n)\omega_{sn}^2\omega_{bn}^2+\Pi_n^2\omega_{bn}^4}.\end{aligned} \tag{A.10}$$

These two expressions can be used to frame ω_{bn}^2 as follows:

$$\begin{aligned}&\frac{1}{2\Psi_n}\left[\omega_{sn}^2+\Pi_n\omega_{bn}^2-\sqrt{\omega_{sn}^4+2(\Pi_n-2\Psi_n)\omega_{sn}^2\omega_{bn}^2+\Pi_n^2\omega_{bn}^4}\right]\\&\quad<\omega_{bn}^2<\frac{1}{2\Psi_n}\left[\omega_{sn}^2+\Pi_n\omega_{bn}^2+\sqrt{\omega_{sn}^4+2(\Pi_n-2\Psi_n)\omega_{sn}^2\omega_{bn}^2+\Pi_n^2\omega_{bn}^4}\right].\end{aligned} \tag{A.11}$$

Finally, from Eqs. (27) and (28), the first inequality required (Eq. (29)) can be obtained:

$$\omega_{nB-0}^2=\omega_{nF-0}^2<\omega_{bn}^2<\omega_{nB+0}^2=\omega_{nF+0}^2.$$

Likewise, upon multiplying Eq. (A.5) by $4\Psi_n/\Pi_n\omega_{sn}^4$, the inequality becomes:

$$4\frac{\Psi_n^2}{\Pi_n^2}\omega_{sn}^4 - 4\frac{\Psi_n}{\Pi_n}\omega_{sn}^4 < 0. \tag{A.12}$$

Adding the term $\omega_{sn}^4 + 2(\Pi_n - 2\Psi_n)\omega_{sn}^2\omega_{bn}^2 + \Pi_n^2\omega_{bn}^4$ to both sides of this inequality, the previous equation becomes

$$\begin{aligned}\omega_{sn}^4 + 2(\Pi_n - 2\Psi_n)\omega_{sn}^2\omega_{bn}^2 + \Pi_n^2\omega_{bn}^4 + 4\frac{\Psi_n^2}{\Pi_n^2}\omega_{sn}^4 - 4\frac{\Psi_n}{\Pi_n}\omega_{sn}^4 \\ < \omega_{sn}^4 + 2(\Pi_n - 2\Psi_n)\omega_{sn}^2\omega_{bn}^2 + \Pi_n^2\omega_{bn}^4,\end{aligned} \tag{A.13}$$

therefore

$$0 < \left(\omega_{sn}^2 + \Pi_n\omega_{bn}^2 - 2\Psi_n\frac{\omega_{sn}^2}{\Pi_n}\right)^2 < \omega_{sn}^4 + 2(\Pi_n - 2\Psi_n)\omega_{sn}^2\omega_{bn}^2 + \Pi_n^2\omega_{bn}^4. \tag{A.14}$$

The square root of the above expression gives the second inequality required (Eq. (30)):

$$\omega_{nB-0}^2 = \omega_{nF-0}^2 < \frac{\omega_{sn}^2}{\Pi_n} < \omega_{nB+0}^2 = \omega_{nF+0}^2.$$

Appendix B. Studies on the modal damping d_{np0}: the case of viscous internal damping

B.1. Damping of the modes nB+

Eq. (27) with ω_{nB+0} can be written as:

$$2\Psi_n\omega_{nB+0}^2 - \omega_{sn}^2 - \Pi_n\omega_{bn}^2 = \sqrt{\omega_{sn}^4 + 2(\Pi_n - 2\Psi_n)\omega_{sn}^2\omega_{bn}^2 + \Pi_n^2\omega_{bn}^4} > 0. \tag{B.1}$$

Since $\omega_{nB+0}^2 > \omega_{bn}^2$ (Eq. (29)), $\pi_n\omega_{nB+0}^2 > \omega_{sn}^2$ (Eq. (30)) and $\omega_{nB+0} < 0$ (backward whirl), from the expression for d_{nB+0} in Eq. (31), the sign of d_{nB+0} can be expressed as follows:

$$d_{nB+0}(\Omega) = d_{in}\frac{\overbrace{\omega_{nB+0}^2 - \omega_{bn}^2}^{>0} + \frac{d_{en}}{d_{in}}\overbrace{(\Pi_n\omega_{nB+0}^2 - \omega_{sn}^2)}^{>0} + \frac{\overbrace{\omega_{nB+0}^2 - \omega_{bn}^2}^{>0}}{-\omega_{nB+0}}\Omega}{2(\underbrace{2\Psi_n\omega_{nB+0}^2 - \omega_{sn}^2 - \Pi_n\omega_{bn}^2}_{>0})}. \tag{B.2}$$

It can then be concluded that d_{nB+0} is positive at null spin speed and that it is a strictly increasing function depending on Ω. $nB+$ modes are therefore always stable.

B.2. Damping of the modes nB−

Eq. (28) with ω_{nB-0} can be written as:

$$2\Psi_n\omega_{nB-0}^2 - \omega_{sn}^2 - \Pi_n\omega_{bn}^2 = -\sqrt{\omega_{sn}^4 + 2(\Pi_n - 2\Psi_n)\omega_{sn}^2\omega_{bn}^2 + \Pi_n^2\omega_{bn}^4} < 0. \tag{B.3}$$

Since $\omega_{nB-0}^2 < \omega_{bn}^2$ (Eq. (29)), $\Pi_n\omega_{nB-0}^2 < \omega_{sn}^2$ (Eq. (30)) and $\omega_{nB-0} < 0$ (backward whirl), from the expression for d_{nB-0} in Eq. (31), the sign of d_{nB-0} can be expressed as follows:

$$d_{nB-0}(\Omega) = d_{in}\frac{\overbrace{\omega_{nB+0}^2 - \omega_{bn}^2}^{<0} + \frac{d_{en}}{d_{in}}\overbrace{(\Pi_n\omega_{nB-0}^2 - \omega_{sn}^2)}^{<0} + \frac{\overbrace{\omega_{nB-0}^2 - \omega_{bn}^2}^{<0}}{-\omega_{nB-0}}\Omega}{2(\underbrace{2\Psi_n\omega_{nB-0}^2 - \omega_{sn}^2 - \Pi_n\omega_{bn}^2}_{<0})}. \tag{B.4}$$

It can then be concluded that d_{nB-0} is positive at null spin speed and that it is a strictly increasing function depending on Ω. $nB-$ modes are therefore always stable.

B.3. Damping of the modes $nF+$

Eq. (27) with ω_{nF+0} can be written as:

$$2\Psi_n\omega_{nF+0}^2-\omega_{sn}^2-\Pi_n\omega_{bn}^2=\sqrt{\omega_{sn}^4+2(\Pi_n-2\Psi_n)\omega_{sn}^2\omega_{bn}^2+\Pi_n^2\omega_{bn}^4}>0. \tag{B.5}$$

Since $\omega_{nF+0}^2>\omega_{bn}^2$ (Eq. (29)), $\Pi_n\omega_{nF+0}^2>\omega_{sn}^2$ (Eq. (30)) and $\omega_{nF+0}>0$ (forward whirl), from the expression for d_{nF+0} in Eq. (31), the sign of d_{nF+0} can be expressed as follows:

$$d_{nF+0}(\Omega)=d_{in}\frac{\overbrace{\omega_{nF+0}^2-\omega_{bn}^2}^{>0}+\frac{d_{en}}{d_{in}}\overbrace{(\Pi_n\omega_{nF+0}^2-\omega_{sn}^2)}^{>0}+\frac{\overbrace{\omega_{nF+0}^2-\omega_{bn}^2}^{<0}}{-\omega_{nF+0}}\Omega}{2\underbrace{(2\Psi_n\omega_{nF+0}^2-\omega_{sn}^2-\Pi_n\omega_{bn}^2)}_{>0}}. \tag{B.6}$$

It can then be concluded that d_{nF+0} is positive at null spin speed and that it is a strictly decreasing function depending on Ω. $nF+$ modes can therefore be unstable. The threshold speed $\Omega_{\text{ths.visc}.nF+}$ can be expressed by solving the equation: $d_{nF+0}(\Omega_{\text{ths.visc}.nF+})=0$.

B.4. Damping of the modes $nF-$

Eq. (28) with ω_{nF-0} can be written as:

$$2\Psi_n\omega_{nF-0}^2-\omega_{sn}^2-\Pi_n\omega_{bn}^2=-\sqrt{\omega_{sn}^4+2(\Pi_n-2\Psi_n)\omega_{sn}^2\omega_{bn}^2+\Pi_n^2\omega_{bn}^4}<0. \tag{B.7}$$

Since $\omega_{nF-0}^2<\omega_{bn}^2$ (Eq. (29)), $\Pi_n\omega_{nF-0}^2<\omega_{sn}^2$ (Eq. (30)) and $\omega_{nF-0}>0$ (forward whirl), from the expression for d_{nF-0} in Eq. (31), the sign of d_{nF-0} can be expressed as follows:

$$d_{nF-0}(\Omega)=d_{in}\frac{\overbrace{\omega_{nF+0}^2-\omega_{bn}^2}^{<0}+\frac{d_{en}}{d_{in}}\overbrace{(\Pi_n\omega_{nF-0}^2-\omega_{sn}^2)}^{<0}+\frac{\overbrace{\omega_{nF-0}^2-\omega_{bn}^2}^{>0}}{-\omega_{nB-0}}\Omega}{2\underbrace{(2\Psi_n\omega_{nF-0}^2-\omega_{sn}^2-\Pi_n\omega_{bn}^2)}_{<0}}. \tag{B.8}$$

It can then be concluded that d_{nF-0} is positive at null spin speed and that it is a strictly decreasing function depending on Ω. $nF-$ modes can therefore be unstable. The threshold speed $\Omega_{\text{ths.visc}.nF-}$can be expressed by solving the equation: $d_{nF-0}(\Omega_{\text{ths.visc}.nF-})=0$.

Appendix C. Studies on the modal damping d_{np0}: the case of hysteretic internal damping

C.1. Damping of the modes $nB+$

Since $\omega_{nB+0}^2>\omega_{bn}^2$ (Eq. (29)), $\Pi_n\omega_{nB+0}^2>\omega_{sn}^2$ (Eq. (30)) and $\omega_{nB+0}<0$ (backward whirl), based on Eqs. (39) and (B.1), the sign of d_{nB+0} can be expressed as follows:

$$d_{nB+0}(\Omega)=\frac{\eta_i\omega_{sn}^2\dfrac{\overbrace{\omega_{nB+0}^2-\omega_{bn}^2}^{>0}}{-\omega_{nB+0}}+d_{en}\overbrace{(\Pi_n\omega_{nB+0}^2-\omega_{sn}^2)}^{>0}}{2\underbrace{(2\Psi_n\omega_{nB+0}^2-\omega_{sn}^2-\Pi_n\omega_{bn}^2)}_{>0}}. \tag{C.1}$$

It can then be concluded that d_{nB+0} is always positive. $nB+$ modes are therefore always stable.

C.2. Damping of the modes nB−

Since $\omega_{nB-0}^2 < \omega_{bn}^2$ (Eq. (29)), $\Pi_n \omega_{nB-0}^2 < \omega_{sn}^2$ (Eq. (30)) and $\omega_{nB-0} < 0$ (backward whirl), based on Eqs. (39) and (B.3), the sign of d_{nB-0} can be expressed as follows:

$$d_{nB-0}(\Omega) = \frac{\eta_i \omega_{sn}^2 \overbrace{\dfrac{\omega_{nB-0}^2 - \omega_{bn}^2}{-\omega_{nB-0}}}^{<0} + d_{en} \overbrace{(\Pi_n \omega_{nB-0}^2 - \omega_{sn}^2)}^{<0}}{2(\underbrace{2\Psi_n \omega_{nB-0}^2 - \omega_{sn}^2 - \Pi_n \omega_{bn}^2}_{<0})}. \tag{C.2}$$

It can then be concluded that d_{nB-0} is always positive. $nB-$ modes are therefore always stable.

C.3. Damping of the modes nF+

Since $\omega_{nF+0}^2 > \omega_{bn}^2$ (Eq. (29)), $\Pi_n \omega_{nF+0}^2 > \omega_{sn}^2$ (Eq. (30)) and $\omega_{nF+0} > 0$ (forward whirl), the sign of d_{nF+0} in the subcritical range based on Eqs. (40) and (B.5) can be expressed as follows:

$$d_{nF+0.sub}(\Omega) = \frac{\eta_i \omega_{sn}^2 \overbrace{\dfrac{\omega_{nF+0}^2 - \omega_{bn}^2}{\omega_{nF+0}}}^{>0} + d_{en} \overbrace{(\Pi_n \omega_{nF+0}^2 - \omega_{sn}^2)}^{>0}}{2(\underbrace{2\Psi_n \omega_{nF+0}^2 - \omega_{sn}^2 - \Pi_n \omega_{bn}^2}_{>0})} \tag{C.3}$$

and in the supercritical range based on Eqs. (41) and (B.5)

$$d_{nF+0.sup}(\Omega) = \frac{\eta_i \omega_{sn}^2 \overbrace{\dfrac{\omega_{nF+0}^2 - \omega_{bn}^2}{-\omega_{nF+0}}}^{<0} + d_{en} \overbrace{(\Pi_n \omega_{nF+0}^2 - \omega_{sn}^2)}^{>0}}{2(\underbrace{2\Psi_n \omega_{nF+0}^2 - \omega_{sn}^2 - \Pi_n \omega_{bn}^2}_{>0})}. \tag{C.4}$$

It can then be concluded that d_{nF+0} is positive in the subcritical range and that it can become negative in the supercritical range if

$$\eta_i \omega_{sn}^2 \frac{\omega_{nF+0}^2 - \omega_{bn}^2}{-\omega_{nF+0}} + d_{en}(\Pi_n \omega_{nF+0}^2 - \omega_{sn}^2) < 0. \tag{C.5}$$

In this case, this $nF+$ mode will always be unstable in the supercritical range.

C.4. Damping of the modes nF−

Since $\omega_{nF-0}^2 < \omega_{bn}^2$ (Eq. (29)), $\Pi_n \omega_{nF-0}^2 < \omega_{sn}^2$ (Eq. (30)) and $\omega_{nF-0} > 0$ (forward whirl), the sign of d_{nF-0} in the subcritical range based on Eqs. (40) and (B.7) can be expressed as follows:

$$d_{nF-0.sub}(\Omega) = \frac{\eta_i \omega_{sn}^2 \overbrace{\dfrac{\omega_{nF-0}^2 - \omega_{bn}^2}{\omega_{nF-0}}}^{<0} + d_{en} \overbrace{(\Pi_n \omega_{nF-0}^2 - \omega_{sn}^2)}^{<0}}{2(\underbrace{2\Psi_n \omega_{nF-0}^2 - \omega_{sn}^2 - \Pi_n \omega_{bn}^2}_{<0})} \tag{C.6}$$

and in the supercritical range based on Eqs.(41) and (B.7)

$$d_{nF-0.sup}(\Omega)=\frac{\eta_i\omega_{sn}^2\overbrace{\frac{\omega_{nF-0}^2-\omega_{bn}^2}{-\omega_{nF-0}}}^{>0}+d_{en}\overbrace{(\Pi_n\omega_{nF-0}^2-\omega_{sn}^2)}^{<0}}{\underbrace{2(2\Psi_n\omega_{nF-0}^2-\omega_{sn}^2-\Pi_n\omega_{bn}^2)}_{<0}}. \tag{C.7}$$

It can then be concluded that d_{nF-0} is positive in the subcritical range and that it can become negative in the supercritical range if

$$\eta_i\omega_{sn}^2\frac{\omega_{nF-0}^2-\omega_{bn}^2}{-\omega_{nF-0}}+d_{en}(\Pi_n\omega_{nF-0}^2-\omega_{sn}^2)>0. \tag{C.8}$$

In this case, this $nF-$ mode will always be unstable in the supercritical range.

References

[1] R.D. Adams, Damping properties analysis of composites, *Engineering Material Handbook*, Vol. 1, ASME, 1987, pp. 206–217.
[2] B.J. Lazan, *Damping of Materials and Members in Structural Mechanics*, Pergamon Press, Oxford, 1968.
[3] M. Darlow, E. Zorzi, *Mechanical Design Handbook for Elastomers*, NASA-CR-3423, 1981.
[4] J.T. Sawicki, G. Genta, Modal uncoupling of damped gyroscopic systems, *Journal of Sound and Vibration* 244 (2001) 431–451.
[5] H.L. Wettergren, On the behavior of material damping due to multi-frequency excitation, *Journal of Sound and Vibration* 206 (1997) 725–735.
[6] G. Genta, On a persistent misunderstanding of the role of hysteretic damping in rotordynamics, *Journal of Vibration and Acoustics* 126 (3) (2004) 459–461.
[7] G. Genta, *Dynamics of Rotating Systems*, Springer, New York, 2005.
[8] Z. Guo, R.G. Kirk, Instability boundary for rotor-hydrodynamic bearing systems, part 1: Jeffcott rotor with external damping, *Journal of Vibration and Acoustics, ASME* 125 (2003) 417–427.
[9] R.G. Kirk, E.J. Gunter, The effect of support flexibility and damping on the synchronous response of a single mass flexible rotor, *Journal of Engineering for Industry, ASME* 94 (1) (1972) 221–232.
[10] J.K. Dutt, B.C. Nakra, Stability of rotor systems with viscoelastic supports, *Journal of Sound and Vibration* 153 (1992) 89–96.
[11] J.K. Dutt, B.C. Nakra, Vibration response reduction of a rotor shaft system using viscoelastic polymeric supports, *Journal of Vibration and Acoustics, ASME* 115 (1993) 221–223.
[12] N.H. Shabaneh, J.W. Zu, Dynamic analysis of rotor-shaft systems with viscoelastically supported bearings, *Mechanism and Machine Theory* 35 (2000) 1313–1330.
[13] O. Montagnier, Tubes Composites à Grande Vitesse de Rotation: Analyses Expérimentales et Modélisation, Ph.D. Thesis, University of Marseille, 2005.
[14] O. Montagnier, C. Hochard, Design of high rotation frequency composite tubes, *Proceedings 11th European Conference on Composite Materials*, Rhodes, Greece, 2004.
[15] D. Smith, The motion of a rotor carried by a flexible shaft in flexible bearings, *Proceedings of the Royal Society of London*, 1933, pp. 92–119.
[16] A. Tondl, *Some Problems of Rotor Dynamics*, Czechoslovak Academy of Sciences, Prague, 1965.
[17] E.S. Zorzi, H.D. Nelson, Finite element simulation of rotor-bearing systems with internal damping, ASME, *Journal of Engineering for Power* 99 (1977) 71–76.
[18] H.N. Özgüven, Z.L. Özkan, Whirl speeds and unbalance response of multibearing rotors using finite elements, ASME, *Journal of Vibration, Acoustics, Stress, and Reliability in Design* 106 (1984) 72–79.
[19] D.-M. Ku, Finite element of natural whirl speeds for rotor-bearing systems with internal damping, *Mechanical Systems and Signal Processing* 12 (5) (1998) 599–610.